JOURNAL OF COMPUTATIONAL PHYSICS 122, 367–379 (1995)

A Spine-Flux Method for Simulating Free Surface Flows

F. MASHAYEK AND N. ASHGRIZ

Department of Mechanical and Aerospace Engineering, State University of New York at Buffalo, Buffalo, New York 14260

Received March 31, 1994; revised October 31, 1994

A new technique for the advection of liquid domains with free surfaces is developed. This technique is based on describing the liquid surface by a spine function $h(\alpha, t)$, with α being the angle measured from one axis at time t. After discretization, the spines $h_i(\alpha_i, t_i)$ subdivide the liquid zone into conical subvolumes. The volume of each of the subvolumes is updated using the local velocities at the interface of every two neighboring subvolumes. A technique is developed to calculate the new spines based on the updated subvolumes. The method is referred to as the spine-flux method (SFM) and it is implemented in a Galerkin finite element method with penalty formulation. The problems of drop oscillation and drop collision are utilized to show the accuracy and efficiency of the technique.

1. INTRODUCTION

In a previous paper [1], we introduced a new technique for simulating free surface flows based on the combination of finite element method for solving the governing equations and a flux method for locating the free surface. The technique, which was called the height-flux method (HFM), was useful when the free surface could be defined as a function of one coordinate only (e.g., axial coordinate in axisymmetric flows). Later, HFM was successfully implemented to study the capillary and thermocapillary breakup of liquid jets [2]. In this paper, we present a new technique for handling the free surface flows when the location of the free surface can be specified as a function of an angular coordinate. The technique is described for axisymmetric flows; however, the case of a 2-D Cartesian flow can be treated in the same fashion.

In the numerical study of drop oscillations, a variety of techniques have been utilized which are basically in common use with other free surface flow problems. In general, finite element and finite difference methods are implemented when a study of viscous drop oscillations over a wide range of Reynolds numbers is concerned. However, these methods need to be furnished with some other complementary techniques to follow the motion of the free surface. A commonly used technique is the volume of fluid (VOF) method [3–7], which performs on an Eulerian grid by advecting the volume fraction, f, field. By definition, $f = 1$ for cells full of fluid, $f = 0$ for empty cells, and $0 < f < 1$ for partially filled cells. The f-field is updated at any time step during the computations by using the velocity field and a surface reconstruction scheme. The VOF technique, which was originally developed for finite difference methods, has recently been implemented in finite element methods by Mashayek and Ashgriz [8]. VOF techniques are also useful in simulating the motion of a front when its velocity is specified. For instance Colella *et al.* [9], Henderson *et al.* [10], and Puckett [11] have used the SLIC method to study shock wave refraction. Marcus *et al.* [12] and Henderson *et al.* [13] have implemented the least-squares technique developed by Puckett [14] to study the hyperbolic flows. In this technique the error between the volume fractions given by the true and approximate interfaces are minimized by the least square line fit to a 3×3 cell unit. Another technique which has widely been used with finite difference method is the marker and cell (MAC) method [15–18]. In the MAC method, hundreds of massless marker particles are added to the fluid. These particles are then advected in Lagrangian sense using the average Eulerian velocities in their vicinity.

While finite difference based techniques have been commonly used to simulate large surface deformations including the breakup and merging of liquids, the finite element based techniques have been more common in simulating less complicated surface deformations. The latter performs on either fixed [19] or deforming spatial meshes. Deforming meshes are more popular and are divided into three subcategories. One is based on a three-stage iterative cycle by guessing the location of the free surface, solving the governing equations, and updating the free surface. Iterations are repeated until the difference between the two successively updated free surface locations becomes less than some desired convergence tolerance [20]. The second approach developed by Saito and Scriven [21] and Ettouney and Brown [22] eliminates the iterations by introducing the position of the nodes on the free surface as a degree of freedom. The third technique is the height-flux method (HFM) developed by Mashayek and Ashgriz [1]. In this technique, neither iterations are involved for locating the free surface nor one degree of freedom is added to the set of the unknowns. The free surface is found by using the volume of fluid inside subvolumes which are updated at any time step using the velocity field. The current paper presents a modified version of HFM, where the free

0021-9991/95 $12.00

surface can be represented by an angular coordinate and it is referred to as the spine-flux method (SFM).

The mathematical formulation of the problem and the surface reconstruction technique are described in Section 2. Drop oscillation problem is used in Section 3 to assess the accuracy and efficiency of the SFM. In Section 4, problems with moving center of mass are considered and a technique is presented for coordinate shift that allows the simulation of large surface deformations.

2. SPINE-FLUX METHOD

The idea of using a flux method to reconstruct the free surface is basically driven from the volume of fluid (VOF) technique which is widely used in conjunction with the finite difference technique. A similar technique was also applied to finite element method by Mashayek and Ashgriz [8]. As far as the discretization of the domain is concerned, the technique which is described in this paper is similar to the spine method of Kistler and Scriven [23]. The major difference between the two techniques lies in the way that free surface location is obtained. In the spine method of Kistler and Scriven [23], the free surface is found by solving for the kinematic boundary condition on the free surface coupled with the continuity and momentum equations. In our technique, the free surface is reconstructed from the velocity field and is completely decoupled from the governing equations. Therefore, less computational effort is needed since the number of equations is decreased by one, and more accuracy is achieved by utilizing the entire velocity field instead of the surface velocities only. More computational efficiency is obtained in our technique by implementing a penalty formulation rather than the mixed method which is implemented in spine method. With the penalty formulation, the continuity equation is absorbed in the momentum equation; therefore, the number of equations is again decreased by one. The flux method has the advantage of decoupling the free surface reconstruction technique from the method which is implemented to solve the flow equations.

2.1. *Mathematical Formulation*

We consider the laminar axisymmetric flow of an incompressible Newtonian viscous fluid with constant properties. All lengths and velocities are normalized by characteristic scales L and U, respectively. The governing equations, in nondimensional form, are the continuity and momentum equations:

$$\frac{\partial u}{\partial z}+\frac{1}{r}\frac{\partial}{\partial r}(rv)=0 \tag{1}$$

$$\frac{\partial u}{\partial t}+u\frac{\partial u}{\partial z}+v\frac{\partial u}{\partial r}-\ddot{z}_{CM}=-\frac{\partial p}{\partial z}+\frac{1}{Re}\left[\frac{\partial^2 u}{\partial z^2}+\frac{1}{r}\frac{\partial}{\partial r}\left(r\frac{\partial u}{\partial r}\right)\right] \tag{2}$$

$$\frac{\partial v}{\partial t}+u\frac{\partial v}{\partial z}+v\frac{\partial v}{\partial r}=-\frac{\partial p}{\partial r}+\frac{1}{Re}\left[\frac{\partial^2 v}{\partial z^2}+\frac{1}{r}\frac{\partial}{\partial r}\left(r\frac{\partial v}{\partial r}\right)-\frac{v}{r^2}\right]. \tag{3}$$

Here, u and v are velocities in the axial, z, and radial, r, directions, respectively. Reynolds and Weber numbers are respectively defined as

$$\mathrm{Re}=\frac{\rho UL}{\mu},\quad \mathrm{We}=\frac{\rho U^2 L}{\sigma}, \tag{4}$$

where, ρ, μ, and σ are the density, viscosity, and surface tension of the fluid, respectively. In the study of drops which undergo nonsymmetric oscillations, with respect to the r-axis, the origin of the coordinate system does not necessarily coincide with the center of mass. Therefore, the body force generated by the acceleration of the center of mass has to be included in the momentum equation. However, owing to the axial symmetry, the center of mass always remains on the z-axis and the body force due to the acceleration of the center of mass is only included in the momentum equation in axial direction. This term is shown by $\ddot{z}_{CM}$ in Eq. (2).

Boundary conditions are given by

$$\begin{cases} u = F(z, r) \\ v = G(z, r) \end{cases} \quad \text{on } S_1 \tag{5}$$

$$\begin{cases} \bar{\tau}_{zz}=\left(\dfrac{2}{\mathrm{Re}}\dfrac{\partial u}{\partial z}-p\right)n_z+\dfrac{1}{\mathrm{Re}}\left(\dfrac{\partial u}{\partial r}+\dfrac{\partial v}{\partial z}\right)n_r \\ \bar{\tau}_{rr}=\dfrac{1}{\mathrm{Re}}\left(\dfrac{\partial u}{\partial r}+\dfrac{\partial v}{\partial z}\right)n_z+\left(\dfrac{2}{\mathrm{Re}}\dfrac{\partial v}{\partial r}-p\right)n_r \end{cases} \quad \text{on } S_2, \tag{6}$$

where S_1 and S_2 are parts of the boundary with Dirichlet and Neumann boundary conditions, respectively. $\bar{\tau}_{zz}$ and $\bar{\tau}_{rr}$ denote z and r components of the total surface traction and n_z and n_r denote direction cosines of the unit outer normal to the surface S_2. On the free surface $\bar{\tau}_{zz}$ and $\bar{\tau}_{rr}$ are the components of the surface tension which are inversely proportional to the radius of the curvature of the surface R_c':

$$\begin{cases} \bar{\tau}_{zz}=\dfrac{\sigma/R_c'}{\rho U^2}n_z=\dfrac{1}{\mathrm{We}}\dfrac{1}{R_c}n_z \\ \bar{\tau}_{rr}=\dfrac{\sigma/R_c'}{\rho U^2}n_r=\dfrac{1}{\mathrm{We}}\dfrac{1}{R_c}n_r \end{cases} \tag{7}$$

We assume that the free surface can be represented by a spine function, $h(\alpha, t)$ with α being the angle measured from the z-axis (Fig. 1). Therefore, the radius of curvature is given by (Becker *et al.* [24]).

$$\frac{1}{R_c}=-\frac{h^2+2h_\alpha^2-hh_{\alpha\alpha}}{(h_\alpha^2+h^2)^{1.5}}-\frac{h-\cot\alpha h_\alpha}{h(h_\alpha^2+h^2)^{0.5}} \tag{8}$$

A Galerkin finite element method with penalty formulation is

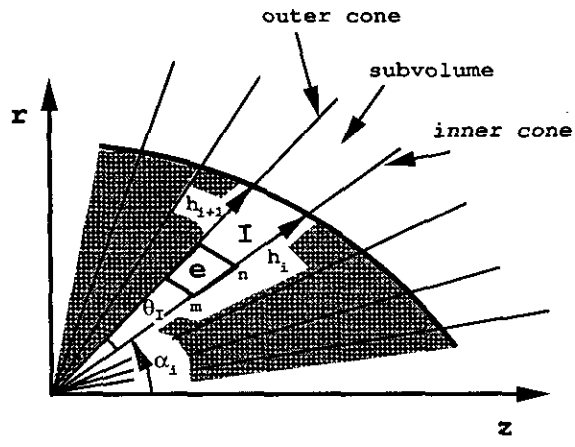

FIG. 1. An axisymmetric fluid domain represented by a spine function. The fluid zone divided into subvolumes represented by their spines and angles.

used to solve Eqs. (1)–(3) subject to boundary conditions (5) and (7). Deforming meshes are required to accommodate the time evolution of the free surface. Here, we allow the motion of the nodes along the spines only according to the following simple rule:

$$h_i(t + \delta t) = ch_i(t). \tag{9}$$

Here the subscript i refers to the node number, and $c = c(\alpha, t)$ is a constant for all the nodes lying on the same spine. The classical finite element formulation, which is based on the Eulerian or fixed mesh, must now be modified to a Lagrangian form in order to consider the motion of the nodes. From a physical point of view, motion of nodes will impose some convective effects on the flow variables. Details of this Lagrangian approach is given by Crank [25].

In order to show how this motion affects the convective terms in Eqs. (2) and (3), consider the axial velocity u at node j. Denote the time rate of change of this velocity, as appears in Eq. (2), with $\partial u/\partial t|_{z,r}$. Then, for the total change of u in the moving frame of reference we can write

$$\left.\frac{\partial u}{\partial t}\right|_j = \left.\frac{\partial u}{\partial t}\right|_{z,r} + \left(\frac{dz}{dt}\right)_j \left(\frac{\partial u}{\partial z}\right)_t + \left(\frac{dr}{dt}\right)_j \left(\frac{\partial u}{\partial r}\right)_t, \tag{10}$$

where the subscript j refers to the derivative in the moving frame of reference. Using Eq. (9) we approximate $(dz/dt)_j$ and $(dr/dt)_j$ with a backward finite difference in terms of c. Therefore,

$$\left.\frac{\partial u}{\partial t}\right|_{z,r} = \left.\frac{\partial u}{\partial t}\right|_j - \frac{c-1}{\delta t} z_j \left(\frac{\partial u}{\partial z}\right)_j - \frac{c-1}{\delta t} r_j \left(\frac{\partial u}{\partial r}\right)_j. \tag{11}$$

Now, recognizing that $(\partial u/\partial t)|_{z,r}$ is the same as $\partial u/\partial t$ of Eq. (2), and dropping the subscripts, we can rewrite Eq. (2) in the moving coordinate as

$$\frac{\partial u}{\partial t} + \left(u - \frac{c-1}{\delta t} z\right)\frac{\partial u}{\partial z} + \left(v - \frac{c-1}{\delta t} r\right)\frac{\partial u}{\partial r} - \ddot{z}_{CM} = -\frac{\partial p}{\partial z} + \frac{1}{\mathrm{Re}}\left[\frac{\partial^2 u}{\partial z^2} + \frac{1}{r}\frac{\partial}{\partial r}\left(r\frac{\partial u}{\partial r}\right)\right]. \tag{12}$$

With a similar argument for the radial momentum equation, one can show that

$$\frac{\partial v}{\partial t} + \left(u - \frac{c-1}{\delta t} z\right)\frac{\partial v}{\partial z} + \left(v - \frac{c-1}{\delta t} r\right)\frac{\partial v}{\partial r} = -\frac{\partial p}{\partial r} + \frac{1}{\mathrm{Re}}\left[\frac{\partial^2 v}{\partial z^2} + \frac{1}{r}\frac{\partial}{\partial r}\left(r\frac{\partial v}{\partial r}\right) - \frac{v}{r^2}\right]. \tag{13}$$

In the calculations, c is approximated as the ratio of $h_i(t)$ to $h_i(t - \delta t)$. Our experience shows that in general c is very close to unity and varies very slightly with time. Therefore, this approximation does not introduce any noticeable error in the results. Details of the finite element formulation are given in Mashayek and Ashgriz [1] and will not be repeated here.

2.2. *Free Surface Determination*

Consider the free surface shown in Fig. 1 (thicker line) on an axisymmetric r–z plane. The volume underneath the free surface is divided into smaller subvolumes. These subvolumes are separated by spines in projected r–z plane and their volumes are inscribed between cones which all have their vertices at the origin. Attributed to each subvolume are an angle θ_i and two spines h_i and h_{i+1}, as shown in Fig. 1. The angle θ_i is known from the initial setup of the problem. The objective of the present technique is to determine h_i and h_{i+1} for each subvolume as a function of time. In order to find h_i and h_{i+1}, we need to know the volume of fluid in each subvolume, V_I. Consider the subvolume I in Fig. 1 which is surrounded by the so-called inner and outer cones. Knowing $V_I(t)$, we are going to find $V_I(t + \delta t)$ using the velocities u and v in axial and radial directions, respectively. The new volume of fluid in the subvolume is calculated by

$$V_I(t + \delta t) = V_I(t) + \delta V_i - \delta V_{i+1}. \tag{14}$$

Here, δV_i and δV_{i+1} are the volume fluxes passing through the inner and outer cone surfaces, respectively. For the flux across the inner cone we can write

$$\delta V = \int_{A_i} U_\perp \delta t dA, \tag{15}$$

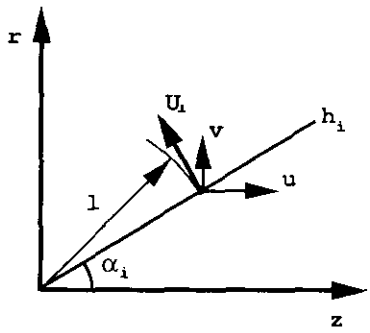

FIG. 2. Velocity perpendicular to a spine, $U_\perp$, is obtained by calculating the components of u and v in the direction normal to that spine.

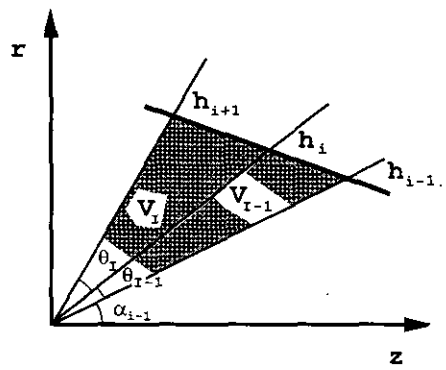

FIG. 3. The part of the interface which is located in two neighboring subvolumes is approximated by a line segment.

where $U_\perp$ is the velocity of the fluid perpendicular to the cone surface, and A is the wetted area on the cone. Let α_i be the angle of the inner cone from the z-axis, then

$$U_\perp = -u \sin \alpha_i + v \cos \alpha_i \tag{16}$$

and

$$dA = 2\pi r dl = 2\pi l \sin \alpha_i \, dl, \tag{17}$$

where l measures the distance from the origin along the spine (Fig. 2). In order to evaluate integral (15), we need to have an expression for the variation of u and v with l. Since the elements employed to discretize the problem domain are linear, therefore, a bilinear approximation for velocity on the element side seems to be quite consistent. Let subscripts m and n refer to the nodal points lying on the spine (Fig. 1). Therefore,

$$u = a_u l + b_u, \quad v = a_v l + b_v \tag{18}$$

with

$$a_u = \frac{u_n - u_m}{l_n - l_m}, \quad a_v = \frac{v_n - v_m}{l_n - l_m},$$

$$b_u = u_m - \frac{u_n - u_m}{l_n - l_m} l_m, \quad b_v = v_m - \frac{v_n - v_m}{l_n - l_m} l_m.$$

Substituting from (16), (17), and (18) into (15), we find for the volume flux along one element side:

$$\delta V_i^{(e)} = 2\pi \sin \alpha_i \delta t \left[\frac{1}{3} (a_v \cos \alpha_i - a_u \sin \alpha_i)(l_n^3 - l_m^3) + \frac{1}{2} (b_v \cos \alpha_i - b_u \sin \alpha_i)(l_n^2 - l_m^2) \right]. \tag{19}$$

Total volume flux along the inner cone, δV_i, is obtained by summing all the elemental fluxes which are given by (19). Same procedure provides δV_{i+1}, and substitution into (14) concludes the calculation of volume of fluid inside subvolume i at time $t + \delta t$.

To complete the surface determination process, we need to solve the inverse problem of determining $h_i(t + \delta t)$, knowing volumes of fluids in subvolumes. In order to find h along a certain spine, we consider two neighboring subvolumes which have that spine in common. Figure 3 shows a schematic of the desired configuration along with the pertinent notations. It is assumed that the part of the interface which is located in these subvolumes can be approximated by a line segment having the equation

$$h = \frac{b}{\cos \alpha - a \sin \alpha}, \tag{20}$$

where α is the angle measured from the z-axis and a and b are two constants yet to be determined. This can be done by writing the equations for the volumes V_{i-1} and V_i using the known angles α_{i-1}, θ_{i-1}, and θ_i,

$$\begin{cases} \dfrac{3}{\pi} V_{i-1} = \dfrac{b^3}{(G_4 - G_3 a)^2 (G_2 - G_1 a)} G_3 G_7 + \dfrac{b^3}{(G_4 - G_3 a)(G_2 - G_1 a)^2} G_1 G_7 \\ \dfrac{3}{\pi} V_i = \dfrac{b^3}{(G_6 - G_5 a)^2 (G_4 - G_3 a)} G_5 G_8 + \dfrac{b^3}{(G_6 - G_5 a)(G_4 - G_3 a)^2} G_3 G_8 \end{cases}, \tag{21}$$

where

$$G_1 = \sin \alpha_{i-1}, \quad G_2 = \cos \alpha_{i-1}$$
$$G_3 = \sin(\alpha_{i-1} + \theta_{i-1}), \quad G_4 = \cos(\alpha_{i-1} + \theta_{i-1})$$
$$G_5 = \sin(\alpha_{i-1} + \theta_{i-1} + \theta_i), \quad G6 = \cos(\alpha_{i-1} + \theta_{i-1} + \theta_i)$$
$$G_7 = \sin \theta_{i-1}, \quad G_8 = \sin \theta_i.$$

are known constants. Equations (21) provide a system of two equations for two unknowns a and b. To solve for a and b, we eliminate b^3 and obtain a cubic equation for a,

$$C_0 a^3 + C_1 a^2 + C_2 a + C_3 = 0, \tag{22}$$

where

$$C_0 = -2G_1^2 G_3 G_5 G_8 V_{i-1} + 2G_1 G_3 G_5^2 G_7 V_i$$
$$C_1 = (G_1^2 G_4 G_5 G_8 + 4G_1 G_2 G_3 G_5 G_8 + G_1^2 G_3 G_6 G_8) V_{i-1}$$
$$- (G_2 G_3 G_5^2 G_7 + 4G_1 G_3 G_5 G_6 G_7 + G_1 G_4 G_5^2 G_7) V_i$$
$$C_2 = -2(G_1 G_2 G_4 G_5 G_8 + G_2^2 G_3 G_5 G_8 + G_1 G_2 G_3 G_6 G_8) V_{i-1}$$
$$+ 2(G_2 G_3 G_5 G_6 G_7 + G_1 G_3 G_6^2 G_7 + G_1 G_4 G_5 G_6 G_7) V_i$$
$$C_3 = (G_2^2 G_4 G_5 G_8 + G_2^2 G_3 G_6 G_8) V_{i-1}$$
$$- (G_1 G_4 G_6^2 G_7 + G_2 G_3 G_6^2 G_7) V_i.$$

Notice that for $\alpha_{i-1} = 0$, Eq. (22) is reduced to a quadratic one (i.e., $C_0 = 0$). Once a is found, b is calculated by substitution of a into either of equations (21). Then, substitution of a and b into (20) gives the surface location $h_i(t + \delta t)$ along the common spine between the two neighboring subvolumes.

The end subvolumes need special treatments as the end spines are attached to one subvolume only. For these subvolumes one may use the symmetry of the shape and find the height along the axis. For instance, along the z-axis, where $\alpha = 0$, the location of the free surface is given by

$$h_1 = \left(\frac{3V_1}{\pi \tan^2 \theta_1}\right)^{1/3}, \tag{23}$$

where subscript 1 refers to first subvolume which is attached to the z-axis. If the spine at $\alpha = \pi/2$ is a symmetry axis then

$$h_{N+1} = \left(\frac{3V_N}{2\pi \tan \theta_N}\right)^{1/3}, \tag{24}$$

with N being the total number of subvolumes.

In order to examine the accuracy of the technique, we have reconstructed the surface of an axisymmetric drop whose surface location is known a priori. We chose a spherical drop which is disturbed by a Legendre function of order four as shown in Fig. 5a below. This particular function is chosen because it includes both concave and convex curves with large curvatures. The surface was reconstructed using different numbers of subvolumes, $N = 10$, 20, 30, 40, and 80. For each case the percent relative error was calculated which is defined as

$$\%\text{Error} = \frac{h_{\text{calculated}} - h_{\text{actual}}}{h_{\text{actual}}} \times 100.$$

Figure 4a shows that the surface reconstructed with 10 subvolumes experiences relative errors as large as -3.5%. As expected, concave parts of the surface are reconstructed with negative errors and convex parts with positive errors. In addition, parts of the surface with smaller curvature show less errors

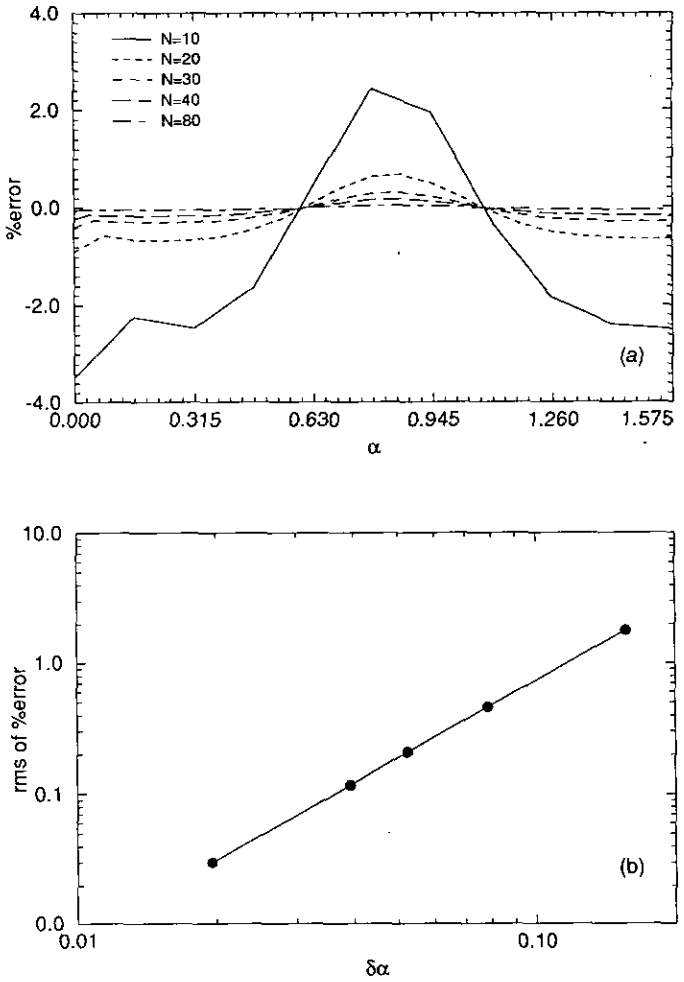

FIG. 4. Accuracy of the technique is tested by reconstructing a known surface using different number of subvolumes. %Error is defined in the text. (a) Variations of the %error versus angular coordinate α for different number of subvolumes N. (b) Variation of root mean square (rms) of %error versus the angular increment $\delta\alpha$, on a log–log plot.

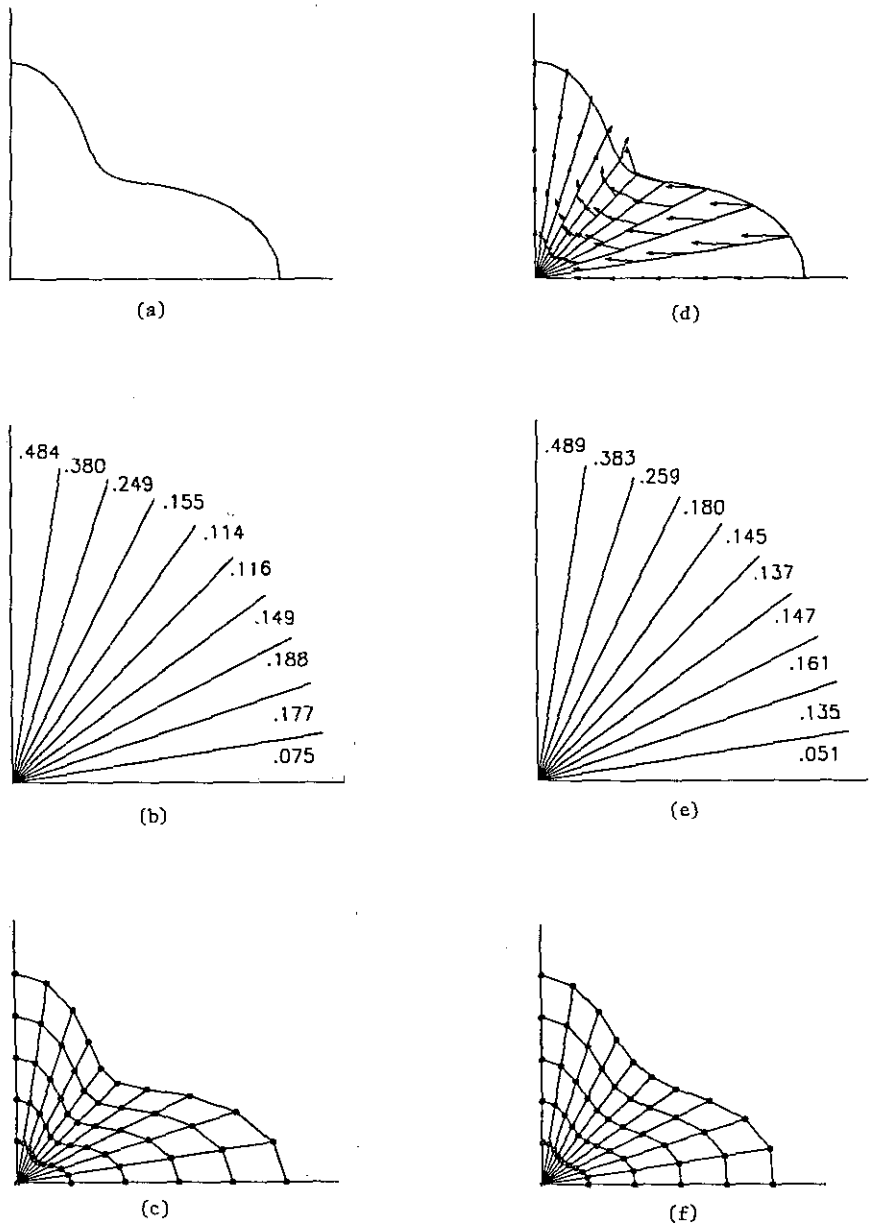

FIG. 5. Illustration of the steps taken in the technique: (a) definition of the initial surface shape, (b) subdivision of the domain into subvolumes and description of the subvolume quantity, (c) mesh generation, (d) calculation of the velocity field, (e) advection of the liquid and calculation of the new subvolume quantities, and (f) reconstruction of the new surface and finite element mesh.

than parts with higher curvature. As the number of subvolumes is increased the accuracy of the surface reconstruction is improved substantially such that with $N = 20$ the maximum relative error drops below 0.9%. Acceptable accuracies are obtained with $N = 30$ and 40 and very good agreement is achieved when 80 subvolumes are used. In order to obtain a more quantitative assessment of the accuracy of this technique, in Fig. 4b we have shown the variation of root mean square (rms) of %error versus the angular increment $\delta\alpha$ ($= \pi/2N$), on a log–log plot. It is clearly seen that the variation is linear with a slope of 1.98. Therefore, the rms of the %error varies proportional to $(\delta\alpha)^{1.98}$ which indicates that SFM is second order accurate in surface reconstruction.

The sequence of operations involved in SFM is summarized in Fig. 5. The initial configuration is shown in Fig. 5a. The volume is divided into 10 subvolumes and fluid volume in each of these subvolumes is calculated by integrating the initial surface function. The amount of fluid inside each subvolume is shown in Fig. 5b. Then, the surface reconstruction technique is invoked and the finite element mesh corresponding to the

reconstructed surface is generated by subdividing the height along each spine into predefined ratios (Fig. 5c). Next, the velocity field is updated by the finite element method. The velocity vectors are shown in Fig. 5d and are used to calculate the new fluid volume in each subvolume (Fig. 5e). It should be mentioned that in order to obtain larger surface motions we have considered an initial horizontal velocity in the negative z direction. The new surface has been reconstructed and shown in Fig. 5f along with the corresponding finite element mesh. This concludes the first time step in the simulation and in the continuation, stages shown in Figs. 5d–5f are repeated for each time step.

3. DROP OSCILLATION

The purpose of this section is two-fold. On one hand, we wish to provide sufficient evidence to reveal the accuracy and efficiency of the technique by comparing the results of our simulations to those of other investigators. On the other hand, a brief case study of oscillations of a liquid drop subject to different initial surface perturbations and various Re numbers are provided. The accuracy of the technique is also examined by comparing the results obtained on successively refined finite element meshes.

For the drop oscillation problem, the characteristic length is the radius of unperturbed spherical drop. Drops are released with a zero velocity field ($u = v = 0$); therefore, to obtain the characteristic velocity, we set We = 1. Consequently, the Re number is calculated using the characteristic length and velocity. Two types of initial surface perturbations are considered here. One is an ellipsoid shape,

$$r_0(\alpha) = \frac{\hat{a}\hat{b}}{[(\hat{a}\sin\alpha)^2 + (\hat{b}\cos\alpha)^2]^{1/2}} \quad \text{at} \quad t = 0, \qquad (25)$$

where $\hat{a}$ and $\hat{b}$ are the nondimensional diameters of ellipsoid in z and r directions, respectively. The angle α is measured from z-axis in the r–z plane of the cylindrical coordinates. Considering volume conservation, $\hat{a}$ and $\hat{b}$ are related by $\hat{a}\hat{b}^2 = 1$; therefore, $\hat{a} = s^{2/3}$ and $\hat{b} = s^{-1/3}$ where $s \approx \hat{a}/\hat{b}$. The second perturbation is proportional to the second spherical harmonic:

$$r_0(\alpha) = R_0[1 + \varepsilon_0 P_2(\cos\alpha)] \quad \text{at} \quad t = 0 \qquad (26)$$

Here ε_0 is the amplitude of the initial disturbance and

$$R_0 = \left(\frac{35}{35 + 21\varepsilon_0^2 + 2\varepsilon_0^3}\right)^{1/3}$$

is used to keep the volume of the drop constant when ε_0 is varied. $P_2(\cos\alpha)$ is the Legendre polynomial.

As a first check on the accuracy of the technique, we simulated the small amplitude oscillations of drop with Re = 100. The period of the oscillation can be compared with the analytical results of Prosperetti [26] who studied the small amplitude oscillations of viscous drops as an initial value problem. Period of oscillation obtained from our simulation for a drop initially perturbed with the second spherical harmonic at $\varepsilon_0 = 0.01$ is 2.2232. This value compares very well with 2.2218 which is predicted by Prosperetti's theory.

TABLE I
The Effect of Mesh Refinement on the Accuracy of the Results

Mesh	τ_s	$\hat{a}$	$\hat{b}$	s
22 × 7	2.4180	1.44259	0.81234	1.77583
26 × 7	2.4225	1.44771	0.81368	1.77922
30 × 9	2.4270	1.45048	0.81465	1.78050

Next, we consider an ellipsoid perturbation with $s = 2$ and Re = 100. This Re number (along with We = 1) corresponds to a spherical water drop with radius of 150 μm. The properties used for water are $\rho = 10^3$ kg/m^3, $\nu = 10^{-6}$ m^2/s, and $\sigma = 0.067$ N/m. In order to analyze the accuracy, simulations of the first period were performed on three different meshes. Table I shows the results of simulations for 22 × 7, 26 × 7, and 30 × 9 element meshes (smaller number is the number of elements in radial direction) using a time step $\delta t = 0.0015$. The period of first oscillation, τ_s, was calculated as the interval between the two maxima observed in time variations of s. Results show that the difference between τ_s obtained by a 22 × 7 mesh and that of the 30 × 9 mesh is less than 0.37%, while the total number of unknowns has been decreased by 69%. It is important to notice the very small sensitivity of the results to the decrease of number of elements in peripheral direction, since this also affects the accuracy of the surface reconstruction technique due to the decrease of number of subvolumes. Values obtained for $\hat{a}$, $\hat{b}$, and s at the end of the first period are also in very good agreement for different meshes.

More simulations were carried out for the same drop ($s = 2$) at lower Re (Re = 1, 3, 10, and 30) and for longer times to see the damping effects of the viscosity. In Fig. 6, we have shown variations of s with time for different Re. It is clearly seen that as the Re is decreased oscillations of the drop damps out faster. At Re = 1, no oscillation is observed and the nature of oscillation is changed from underdamped to overdamped. This is in agreement with the results of Basaran [27] who reported a critical value for Reynolds number between 1.3 and 1.4 at which this change of nature of oscillations occurs. Similar phenomenon was observed by Ashgriz and Mashayek [28] in the study of oscillations of capillary jets in the stable region. Variations of period of oscillation of the drop versus number of periods is shown in Fig. 7 for Re = 10 and 30. In general, period of oscillation decreases with number of periods; however, the rate of decrease is higher at larger Re number.

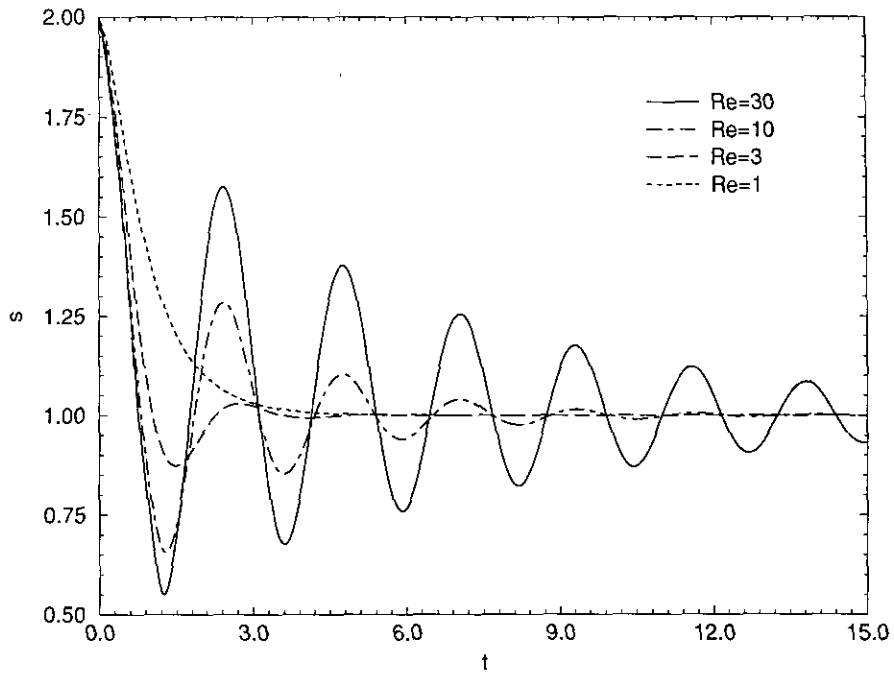

FIG. 6. Oscillations of drops with initial $s = 2$ at different Re numbers. For a drop with Re = 1, no oscillation is observed.

Two large amplitude drop oscillations have also been performed in order to compare the results with those obtained by other investigators. For comparison, we chose one drop with ellipsoid initial deformation with $s = 3$, and one drop with the second spherical harmonic perturbed with $\varepsilon_0 = 0.9$. For these cases, Re was 100. Time evolutions of the shapes of these drops during the first period are shown in Figs. 8 and 9, respectively. These cases have already been simulated by Basaran [27] (his Figs. 6 and 3, respectively) using a very accurate finite element method. To perform these simulations, he implemented a 16×8 quadrilateral finite element mesh (his Mesh III) with a total of unknowns equal to 1308. In our simulations, we employed a 30×9 bilinear element mesh which results in a total of 620 unknowns, which is less than half of that of Basaran's Mesh III. We compared the shape evolutions obtained by the two simulations and observed very good agreements up to the thickness of the lines.

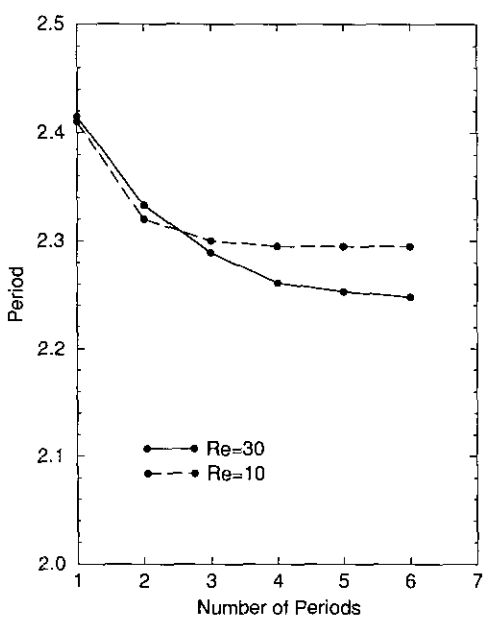

FIG. 7. Period of oscillations as a function of number of periods for drops with initial $s = 2$ and Re = 10 and 30.

In general, oscillation of a drop is governed by competition among kinetic energy, surface energy, and viscous dissipation. At high Re numbers, viscous dissipation is less important and behavior of the drop can be explained by analyzing kinetic and surface energies. As an example for this, consider oscillation of the drop shown in Fig. 8 in time interval $1.0 < t < 1.2$. Figure 8 shows that during this interval the surface of the drop experiences more radial displacement than axial. However, mass conservation considerations require the inverse to happen, since larger volume change is attainable with smaller surface displacement at larger radius. Therefore, it is inferred that the velocity of fluid around the z-axis must have been decreased in this interval. In order to clarify this point, we have plotted the velocity vectors at $t = 1.0$, 1.1, and 1.2 in Fig. 10. On the left, the evolution of the finite element mesh with time is shown. Vectors used for presenting velocities have same scale for $t = 1.0$ and 1.1; however, the scale changes for $t = 1.2$. In Fig.

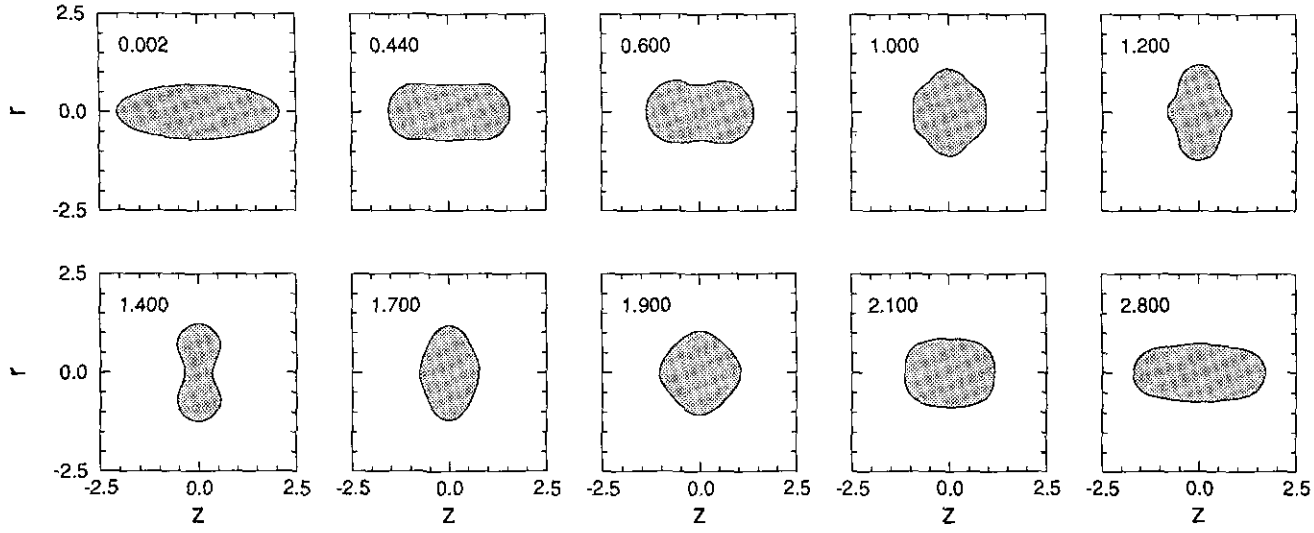

FIG. 8. Time-resolved shape evolutions of an ellipsoid drop with initial $s = 3$ released with zero velocity. Numbers on the figure show the time.

10a, it is seen that a flat region is formed on the drop surface around the z-axis. This results in the decrease of surface curvature and consequently surface energy in this region which necessitates redistribution of the surface energy. Sequences of surface energy redistribution are clearly seen in Figs. 10a–10c. The velocity of the fluid is reduced around the z-axis while other parts of the surface move faster. As a result of this, a region with high curvature is formed which is now capable of pushing the fluid toward the center of the drop.

4. USING COORDINATE SHIFT TO SIMULATE LARGE SURFACE DEFORMATIONS

A shortcoming associated with SFM (or spine methods in general) arises when problems with nonsymmetric surface evolutions, with respect to r-axis, are encountered. A typical case is the oscillation of a drop whose surface is initially perturbed with an odd spherical harmonic. Another case is the collision of two non-equal size liquid drops. In these problems, the nonsymmetric evolution of the surface may result in a surface shape that becomes very close to the origin of the coordinate frame from one side. In more severe cases the surface may even pass the origin which results in a situation that there is no unequivocal radial direction. Obviously, when this happens, calculations become considerably less accurate, if it is not impossible, unless a measure is adopted to shift the coordinate from its original position. One way to accomplish this task is to consider an artificial motion of the liquid domain relative to the coordinate which is guaranteed not to affect the solution due

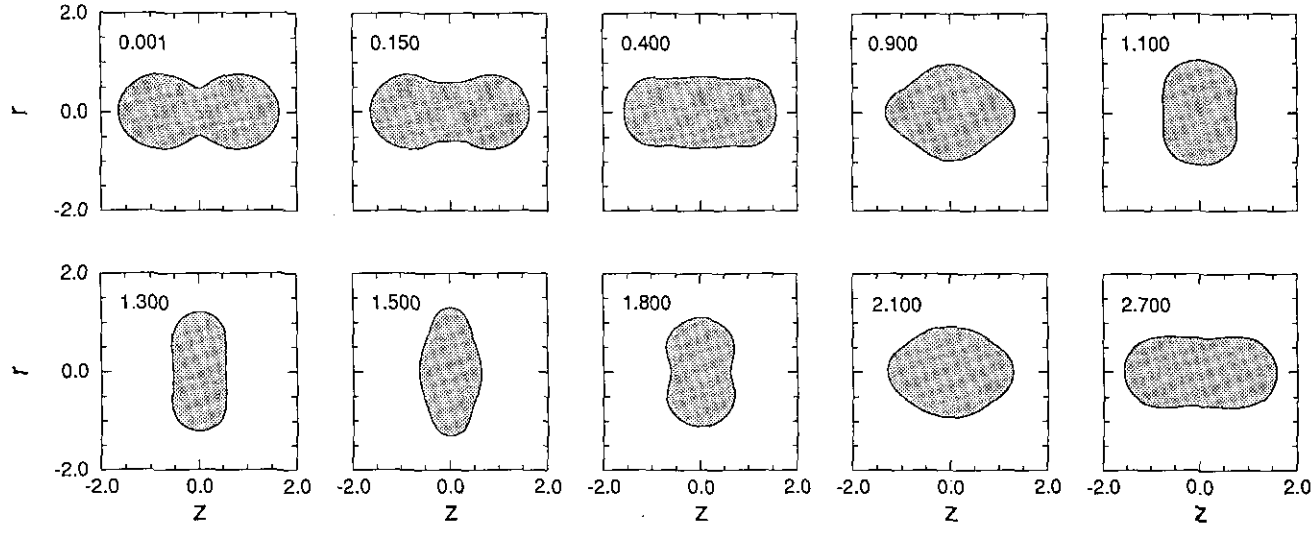

FIG. 9. Time-resolved shape evolutions for a drop released from the second spherical harmonic with $\varepsilon_0 = 0.9$. Numbers on the figure show the time.

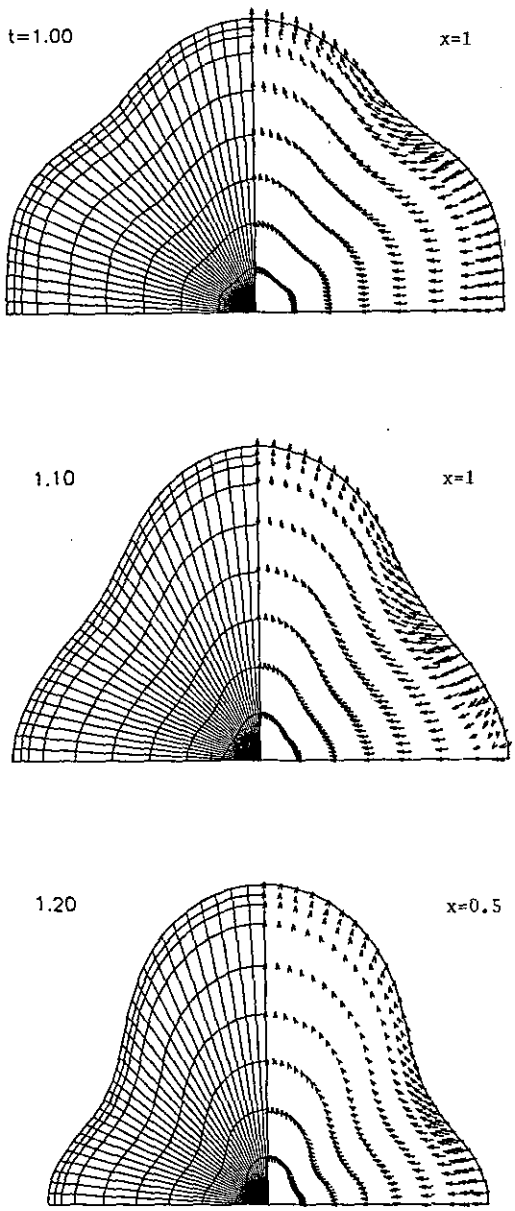

FIG. 10. Velocity vector plots and finite element meshes for the drop shown in Fig. 7 at times $t = 1.0$, 1.1, and 1.2. x is the vector scale for velocity with respect to the velocities at $t = 1.0$.

to the invariance of Navier–Stokes equations under a Galilean transformation. Therefore, initially a constant axial velocity is added to the liquid velocity field which results in a relative motion of the liquid domain with respect to the coordinate. The magnitude of this velocity is chosen such that it results in a proper coordinate shift during the expected time interval. Once the coordinate is reached to its desired position the constant velocity is subtracted from the velocity field.

In order to clarify this procedure consider the problem of collision of two nonequal size liquid drops. We can only consider the head-on collision of two drops which allows an axisymmetric simplification. We are also limited to surface deformations which do not result in the so-called double definition of the surface along a spine (i.e., a spine can not intersect the surface at more than one point, otherwise the simulation fails). Figure 11a shows a schematic of the initial setup of the problem. The initial location of the coordinate has to be close to the contact plane of two drops in order to have a suitable distribution of subvolumes and to prevent the double-definition. However, this location of the coordinate is far from the center of mass. Considering that at long times the coalesced drop is going to oscillate about the center of mass, the initial position of the coordinate will not be a proper choice for long time oscillations of the liquid drop (Fig. 11b). To remedy this mismatch of the coordinate frame and the liquid motion, one may decide to stop the simulation at the situation shown in Fig. 2b and restart the calculations with the coordinate position shown in Fig. 2c. However, this would require recalculation of the subvolumes

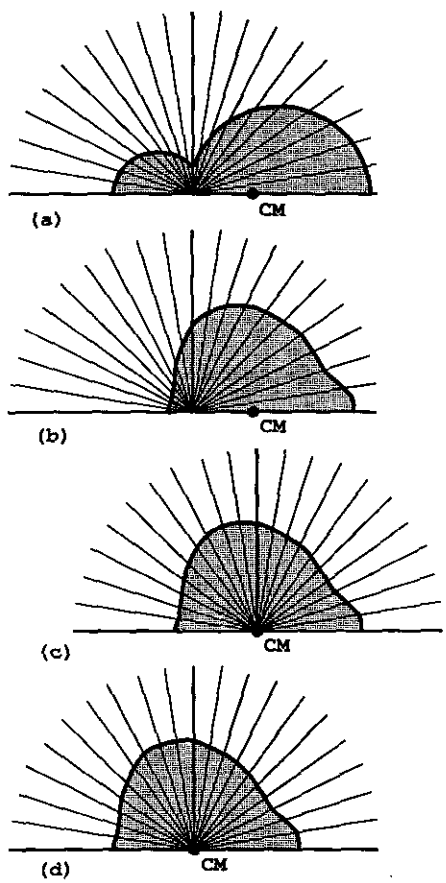

FIG. 11. The coordinate shift procedure is explained by using schematics of a drop collision problem. (a) In the initial setup of the problem the coordinate is located on the contact surface of drops which does not coincide with the center of mass (CM) of the system. (b) After coalescence the liquid drop oscillates about the center of mass which results in improper discretization of the liquid domain into subvolumes. To achieve the proper discretization, either (c) the coordinate origin is shifted to the center of mass or (d) the center of mass is shifted to the origin of the coordinate system.

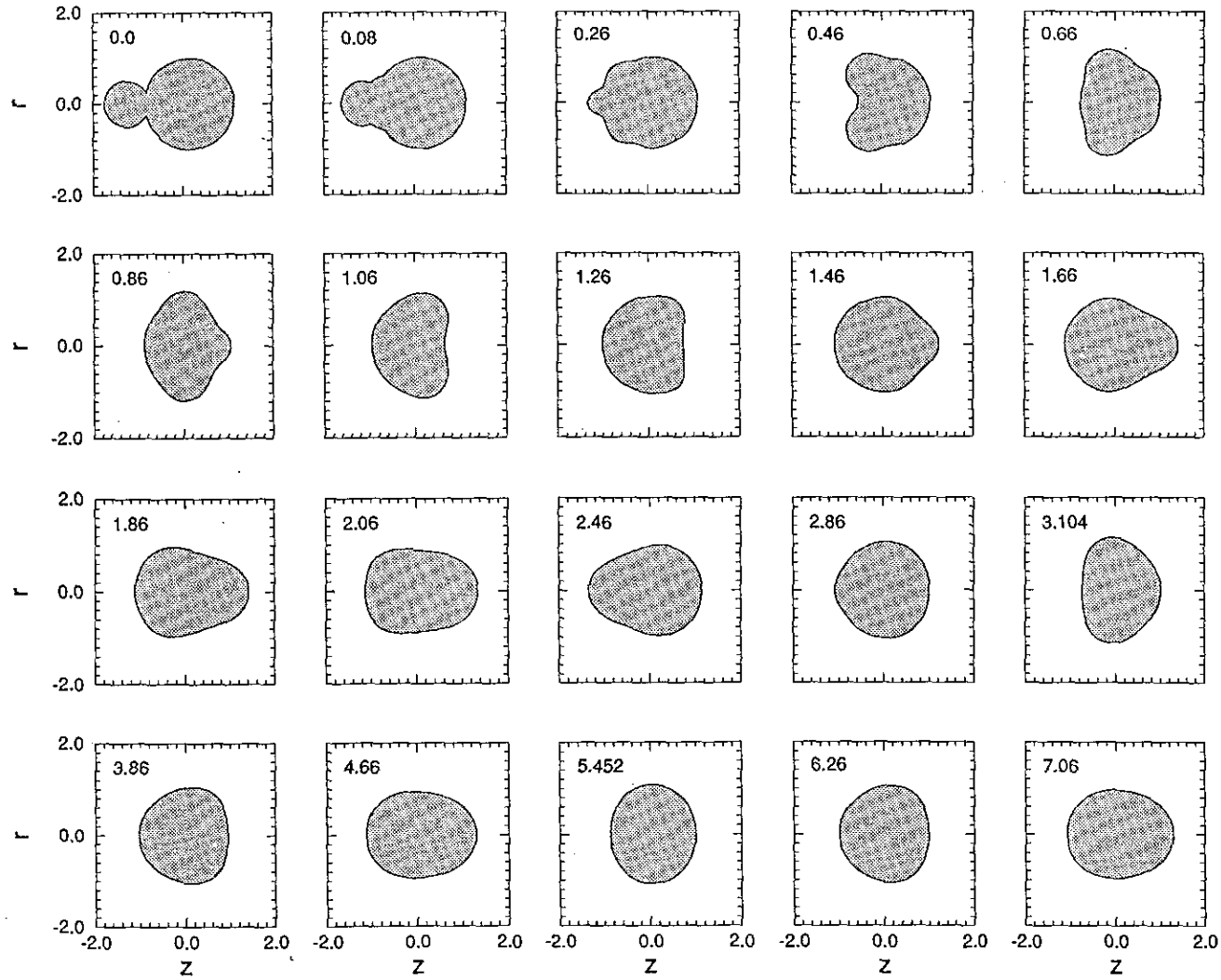

FIG. 12. Time evolutions of the surface of two coalesced drops with We = 1 and Re = 50. The relative impact velocity is 2 and the drop size ratio is 0.5. The numbers on the figure show the time.

based on the new location of the drop, and generation of a new finite element mesh. It is also required that the velocities are interpolated to the new node positions. This procedure is tedious and results in the loss of accuracy. An alternative to this lengthy procedure is to move the liquid domain with respect to the coordinate with a constant velocity, starting at time $t = 0$. Once the center of mass of the liquid coincides with the origin of the coordinate, further relative motion is eliminated by subtracting the constant velocity from the velocity field. The result is seen in Fig. 11d.

A typical case of non-equal size drop collision for We = 1 and Re = 50 is shown in Fig. 12. The nondimensional relative impact velocity is 2 and the ratio of the radii of the two drops is 0.5. The length scale for this problem is the radius of the larger drop. An initial contact between the drops has to be considered in order to implement SFM to this problem which is shown in Fig. 12 at $t = 0$. Notice that the velocity of the center of mass changes with time. Therefore, the coordinate frame which is initially coincided with the center of mass will have a different location than the instantaneous center of mass. However, the deviation is small compared to the drop radius and a coordinate frame moving with the initial velocity of the center of mass is suitable for long time simulations. All the results are shown on a coordinate frame which is moving with the initial velocity of the center of mass. The body force produced by acceleration of the center of mass has been included in this problem as explained in Section 2. In order to accomplish the coordinate shift from the initial contact plane to the center of mass, a constant negative axial velocity of magnitude unity is added to the initial velocities of the drops which are calculated from the relative impact velocity in a coordinate moving with initial velocity of the center of mass. Approximately, at time $t = 0.81$ the center of mass coincides with the coordinate origin and the constant velocity is subtracted from the velocity field.

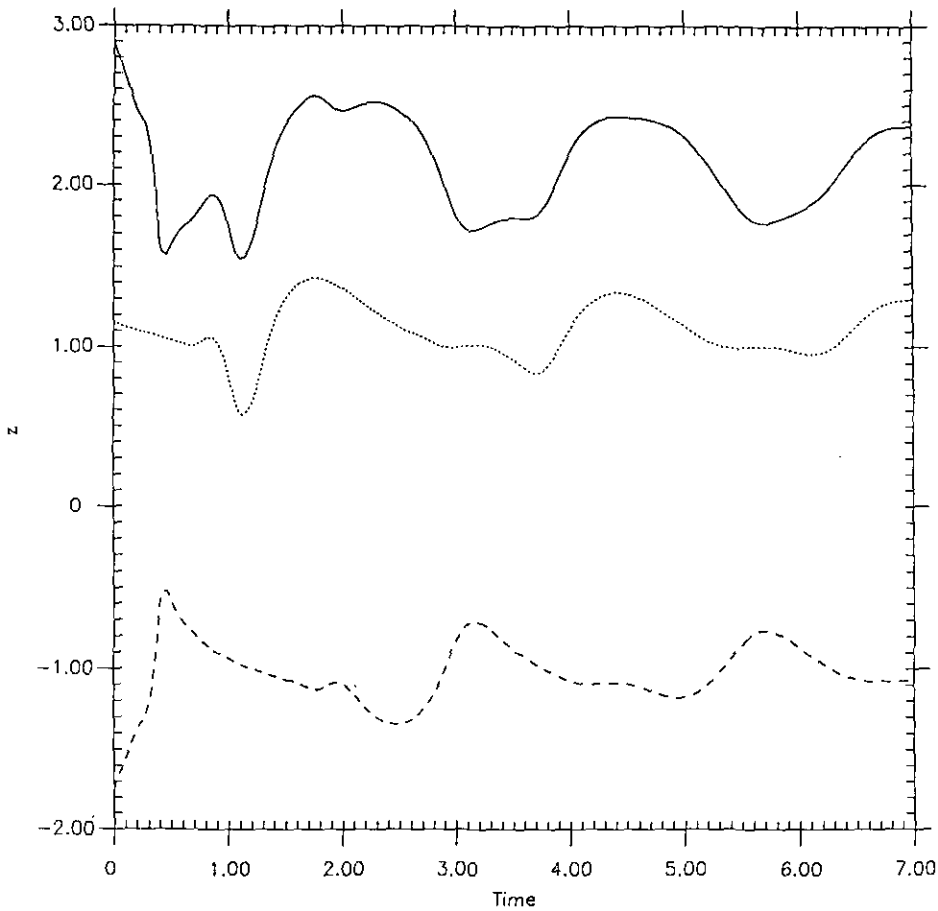

FIG. 13. Variation of the location of surface points on the z-axis with time. (···) belongs to the point on the larger drop and (- - -) belongs to the point on the smaller drop. The distance between the two points is shown by (—).

In Fig. 13, we have plotted the position of the two surface points which are located on the z-axis. The variation of the distance between these points with time is also shown on the figure. Notice that no discontinuity in these curves is observed at $t = 0.81$ which indicates the smooth transition. The curves of Fig. 13 show that the two end points of the coleasced drop oscillate with almost same period, but with a phase shift. The amplitude of the oscillation is decreased with time due to the presence of viscosity and as it is seen in Fig. 12, at longer times the drop approaches to a spherical shape.

5. CONCLUSION

A spine-flux-method (SFM) has been developed for simulating the free surface flow. This method, which is based on describing the free surface by a spine function h, discretizes the liquid zone into conical subvolumes. The volume of each of the subvolumes is updated using the local velocities at the interface of every two neighboring subvolumes. Then, the new spines are calculated using the updated subvolumes. A Galerkin finite element method with penalty formulation is implemented for solving the momentum equations.

In general, three different aspects are distinguishable in a free surface flow code: (1) Velocity field calculation, (2) surface reconstruction, and (3) curvature calculations. Although, these aspects are highly coupled, improvement of any of the three, in a consistent manner, may result in the enhancement of the performance of the code. In comparison to the "traditional" finite difference based VOF methods, the technique presented in this paper provides higher order of accuracy in all of the above mentioned parts. The velocity calculations at the interface are more accurate since the finite element method eliminates the need for interpolation or extrapolation schemes. Surface reconstruction also provides higher accuracy, as discussed in section 2.2. The major source of the error in the calculation of the curvature in VOF techniques is the difficulty in describing a constant base for the height calculations. This defficiency has been overcome in the spine-flux method by using a constant base (i.e., the origin of the coordinate system) for the determination of the height at various locations on the free surface. Therefore, since the performance of the code has been consistently upgraded in every aspects, the overall accuracy increases accordingly.

In addition, the spine-flux method presented here has the

advantage over the conventional spine methods in that the number of equations to find the location of the free surface is decreased by one, therefore, resulting in a more computationally efficient method. Also it utilizes the entire velocity field instead of the surface velocity to advect the interface; therefore, it results in a more accurate surface advection. It is also shown that in problems with a moving center of mass a coordinate shift can be adopted that allows the simulation of large surface deformations. The performance of the technique is examined by simulating several drop oscillation and drop collision problems. Comparisons made with the available analytical and numerical results indicate that a high degree of accuracy is achieved by using relatively coarse meshes.

ACKNOWLEDGMENTS

This work was supported by the Fluid Particulates and Hydraulic Systems Division of NSF under Grant CTS-9011201, and NASA Microgravity program under grant NAG3-1620.

REFERENCES

1. F. Mashayek and N. Ashgriz, *Int. J. Numer. Methods Fluids* **14,** 1035 (1993).
2. F. Mashayek and N. Ashgriz, *J. Fluid Mech.*, **283,** 97 (1995).
3. W. F. Noh and P. Woodward, in *Proceedings of the Fifth International Conference on Numerical Methods in Fluid Dynamics,* edited by A. I. van de Vooren and P. J. Zandbergen. Lecture Notes in Physics, Vol. 59 (Springer-Verlag, New York, 1976), pp. 330–340.
4. B. D. Nichols, C. W. Hirt, and R. S. Hotchkiss, Los Alamos Scientific Lab. Report No. LA8355, 1980.
5. C. W. Hirt and B. D. Nichols, *J. Comput. Phys.* **39,** 201 (1981).
6. N. Ashgriz and J. Y. Poo, *J. Comput. Phys.* **93,** 449 (1991).
7. F. Mashayek and N. Ashgriz, *Int. J. Numer. Methods Fluids* **20,** 1337 (1995).
8. F. Mashayek and N. Ashgriz, *Int. J. Numer. Methods Fluids* **20,** 1363 (1995).
9. P. Colella, L. F. Henderson, and E. G. Puckett, AIAA-89-1973, 426, 1989.
10. L. F. Henderson, P. Colella, and E. G. Puckett, *J. Fluid Mech.* **224,** 1 (1991).
11. E. G. Puckett, in *Multidimensional Hyperbolic Problems and Computations,* edited by J. Glimm and A. J. Majda. The IMA volumes in Mathematics and Its Applications, Vol. 29 (Springer-Verlag, New York), p. 261.
12. D. L. Marcus, E. G. Puckett, J. B. Bell, and J. S. Saltzman, in *Proceedings of the Third International Workshop on the Physics of Compressible Turbulent Mixing, Abbey of Rayaumont, France, June 17–19, 1991.*
13. L. F. Henderson, E. G. Puckett, and P. Colella, in *Proceedings of the second Japan–Soviet Union Joint Symposium on Computational Fluid Dynamics, Tsukuba, Japan, August 27–31, 1990,* Vol. 1, p. 144.
14. E. G. Puckett, in *Proceedings of the 44th International Symposium on Computational Fluid Dynamics, Davis, CA, September 9–12, 1991.*
15. J. E. Welch, F. H. Harlow, J. P. Shannon, and B. J. Daly, Los Alamos Scientific Lab. Report No. LA-3425, 1966.
16. F. H. Harlow and J. F. Welch, *Phys. Fluids* **8,** 2182 (1965).
17. H. Miyata and S. Nishimura, *J. Fluid Mech.* **157,** 327 (1985).
18. H. Miyata, *J. Comput. Phys.* **65,** 179 (1986).
19. K. J. Bathe and M. R. Khoshgoftaar, *Int. J. Numer. Anal. Mech. Geomech.* **3,** 13 (1979).
20. R. I. Tanner, R. E. Nickell, and R. W. Bilger, *Comput. Methods Appl. Mech. and Eng.* **6,** 155 (1975).
21. H. Saito and L. E. Scriven, *J. Comput. Phys.* **42,** 53 (1981).
22. H. Ettouney and R. A. Brown, *J. Comput. Phys.* **49,** 118 (1983).
23. S. F. Kistler and L. E. Scriven, in *Computational Analysis of Polymer Processing,* edited by J. R. A. Pearson and S. M. Richardson (Applied Science Publishers, New York, 1983), p. 243.
24. E. Becker, W. J. Hiller, and T. A. Kowalewski, *J. Fluid Mech.* **231,** 180 (1991).
25. J. Crank, in *Mathematical Methods in Heat Transfer,* edited by R. W. Lewis, K. Morgan, and O. C. Zienkiewicz (Wiley, New York, 1981), p. 177.
26. A. Prosperetti, *J. Fluid Mech.* **100,** 333 (1980).
27. O. A. Basaran, *J. Fluid Mech.* **241,** 169 (1992).
28. N. Ashgriz and F. Mashayek, *J. Fluid Mech.* **291,** 163 (1995).